J Mol Model (2001) 7:216–222
DOI 10.1007/s008940100034

ORIGINAL PAPER

Ahmed S. Shalabi · Khalid M. Eid

F_2-defect-based model for latent image formation and interactions of O, O^- and O^{2-} adsorbates at AgCl and AgBr (001) surfaces: DFT calculations

Received: 7 February 2001 / Accepted: 7 May 2001 / Published online: 11 July 2001

Abstract In an attempt to look for defect-based models for latent image formation, we have examined the reduction and mobility of silver clusters over the F_2-defect-containing surfaces of AgBr and AgCl crystals as well as the interactions of O, O^- and O^{2-} external adsorbates using an embedded cluster model and density functional theory calculations with effective core potentials. The alkali halide clusters were embedded in simulated Coulomb fields that closely approximate the Madelung fields of the host surfaces. The most energetically preferred orientations of silver clusters were associated with the rotational angle θ=30° with an uncertainty of ±2°, 0.05 Å above each surface, internuclear separations of ca. 2.72 and 2.77 Å and activation energy barriers for rotational diffusion of ca. 0.36 and 0.364 eV for AgBr and AgCl, respectively. About 80–83% of the reduction of silver clusters was attributed to the internal structure of the lattice, leaving ca. 17–20% for reduction from external sources such as adsorbates, chemical reducing agents or developers. The contributions to adsorbate–substrate interactions were explainable in terms of surface electrostatic potentials. O, O^- and O^{2-} species adsorb chemically on the defect-containing surfaces. Charge transfer takes place from the surface to oxygen atoms and from the oxygen anions to the surface, confirming the donor–acceptor properties of the title adsorbates in the course of the adsorbate–substrate interactions.

Keywords F_2 model · Latent image · Adsorption · Silver halides · DFT calculations

A.S. Shalabi (✉)
Department of Chemistry, Faculty of Science,
Benha University, Benha, Egypt
e-mail: asshalabi@hotmail.com
Tel.: +20-10-521-1681
Fax: +20-2-418-8738 and +20-13-222-578

K.M. Eid
Department of Physics, Faculty of Education,
Ain Shams University, Cairo, Egypt

Introduction

Silver halides are considered as ionic, as suggested by the position of their component elements in the Periodic Table, by the crystallization of AgBr and AgCl in rock-salt structures and by their electrical conductivity in the solid and molten salts. The special features of silver halides, such as high mobilities of interstitial silver ions and of dislocations lead to technological applications of silver halides in photography. [1, 2] Small silver clusters on the halide surface are proposed to account for the latent image formation, but the details of the process are still being debated. Geometric or steric constraints and/or electronic interactions with the supporting crystal might significantly alter the pattern of s^1 metal clusters of photographic importance. Semiempirical quantum mechanical calculations with varying degrees of sophistication have been directed toward this question. The most extensive are those of Baetzold, [3] in which models of the defect sites of the support have been included. The low jump energy of Ag^+ interstitial ions in silver halides has also been discussed by Jacobs et al. [4] in terms of the quadrupolar deformation of the silver ion in the interstitial position. Of particular interest, Flad et al. investigated latent image formation by carrying out quantum chemical calculations to model the silver halide surface [5] and to examine the adsorption of Ag^+ and Ag on an AgBr (001) surface. [6] To model the silver halide surface, they presented a method to take into account the influence of a silver halide surface on adsorbed silver clusters and suggested a new bromide pseudopotential. To examine the adsorption of Ag^+ and Ag on the (001) AgBr surface, they considered interstitial subsurface sites and incomplete surfaces with ledges and corners. Later, Shelimov et al. [7] carried out ab initio calculations of the geometry, electronic structure, ionization and excitation energies of an Mcenter (F_2-center) on the AgBr (001) surface. They reported that the structure formed in the process of surface reduction may be viewed as an Ag_2 molecule adsorbed on the defect-containing AgBr (001) surface and may become

a primary center for photographic latent image formation.

However, the activation barrier for the rotational diffusion of the adsorbed silver clusters in the (001) plane was not considered. We have therefore examined the mobility of the adsorbed silver clusters on M-defect-containing surfaces of AgBr and AgCl in our attempt to understand the nature of internal reduction by virtue of M-center formation.

Theoretical and experimental studies of adsorption on solid surfaces have become of increasingly importance. [8] This is attributed to the fact that they are related to a variety of technologically significant processes, not least of which are catalysts, corrosion and gas sensors. The chief problem in studying these processes computationally is the treatment of the extended surface when examining a localized phenomenon like chemisorption. [9] For simple systems such as atoms or small molecules interacting on surfaces, it can be feasible to use an extended two-dimensional periodic system and to study an ordered overlayer of adsorbate on the surface. Such examinations have sometimes used slab calculations, [10] although more recently surface embedding is providing a promising route forward. Several theoretical studies have been done to simulate adsorption of simple systems on ionic surfaces. [11] However, alkali halide surfaces are known to be highly stable and the nature of the adsorbate–substrate interaction or charge transfer is not so clear. We have therefore examined the nature of interactions between O, O^- and O^{2-} adsorbates and AgBr and AgCl M defect-containing surfaces as well as the nature of charge transfer from O, O^- and O^{2-} adsorbates – as external reducing agents – to AgBr and AgCl surfaces.

Methods

In cluster calculations, the host surface is represented by only a small number of ions explicitly in three-dimensional space. To represent the Madelung field effects of the remaining crystal, Shelimov et al. [7] used the Evjen method. [12] In this method, the cluster is surrounded by a set of point charges placed at ideal lattice sites. The value of a point charge on the border of this set is 2^{-n}, n being the number of missing nearest neighbors of this charge.

To represent the extended crystal properly, some care needs to be taken in choosing the charges of the point ions, according to the prescription outlined by Harris. [13] For a bulk crystal, the criteria are that there must be no net charge, no net dipole and no net quadrupole in the cluster. For a surface, there is a small dipole induced by surface rumpling; so the criterion of no net dipole does not hold rigorously. [14] The choice of the appropriate charges for the point ions has been discussed for an fcc structure like MgO. [15] Early studies by Kunz et al. [16] and by Colbourn and Mackrodt [17] used clusters that were terminated by full ionic charges. One of the aspects of these calculations (which is most surprising) is that very small clusters – sometimes a single surface ion – can be adequate to represent surface reactivity. This is a consequence of the high degree of localization of the electrons on the ions, and would not hold for materials with any appreciable degree of covalence.

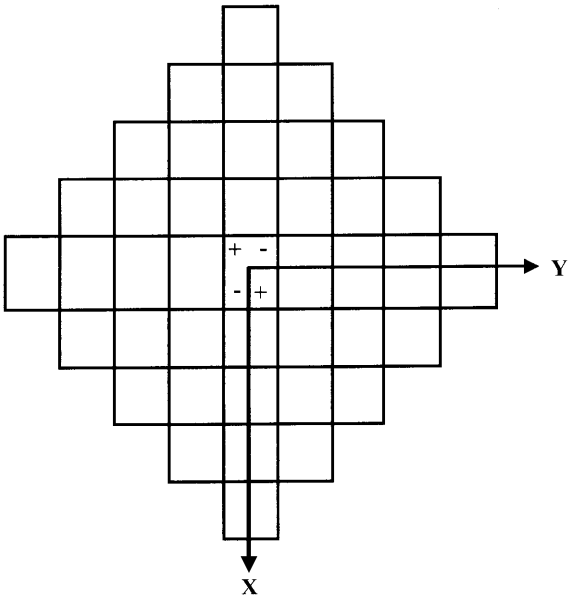

Fig. 1 Representation of the Z=0 plane of the lattice used in the calculations

To simulate the AgBr and AgCl crystals, we follow a procedure previously reported for MgO [18] and LiH. [19] A finite crystal of 288 point charges was first constructed. The Coulomb potential along the X- and Y-axes of this crystal is zero by symmetry as in the host crystal (Fig. 1). The charges on the outer shells listed in Table 1 were then modified to make the Coulomb potential at the four central sites equal to the Madelung potential of the host crystal and to make the eight points with coordinates (0, ±R, ±R) and (±R, 0, ±R), where 2R=2.867 Å for AgBr and 2.755 Å for AgCl, equal to zero, as it should be in the host crystal. With these charges, 0.409283 and 0.800909, the Coulomb potential in the region occupied by the central ions is very close to that in the unit cell of the host crystal. To simulate the AgBr and AgCl surfaces, all charged centers with cartesian coordinates ±X, ±Y and Z=2R, 4R, 6R and 8R were eliminated to generate a surface of 176 charged centers occupying the three-dimensional space ±X, ±Y and –Z=0, 2R, 4R, 6R and 8R. The coordinates of these charged centers are given in Table 1. The metal halide clusters were then embedded within the central region of the crystal surface. All the electrons of the embedded clusters were included in the Hamiltonian of ab initio calculations. Other crystal sites entered the Hamiltonian as point ions.

To include the M-center in the calculations, we considered two electrons trapped in two neighboring anion vacancies along the ⟨110⟩ axis. We then took as our model of the M-center, molecular clusters of silver nuclei at nearest neighbor sites to the two anion vacancies, with n

Table 1 Specification of the finite lattice used for bulk and surface simulation. *R* is half the lattice distance, which is 2.867 Å for AgBr and 2.755 Å for AgCl. *r* is the distance of the appropriate shell from the center of the lattice

r^2/R^2	Coordinates/R^a $\|X\|, \|Y\|, \|Z\|$	Number[a] of centers	Coordinates/R^b $\|X\|, \|Y\|, -Z$	Number[b] of centers	Charge $\|q\|$
2	1 1 0	4	1 1 0	4	1
6	1 1 2	8	1 1 2	4	1
10	3 1 0	8	3 1 0	8	1
14	3 1 2	16	3 1 2	8	1
18	1 1 4	8	1 1 4	4	1
18	3 3 0	4	3 3 0	4	1
22	3 3 2	8	3 3 2	4	1
26	5 1 0	8	5 1 0	8	1
26	3 1 4	16	3 1 4	8	1
30	5 1 2	16	5 1 2	8	1
34	3 3 4	8	3 3 4	4	1
34	5 3 0	8	5 3 0	8	1
38	5 3 2	16	5 3 2	8	1
38	1 1 6	8	1 1 6	4	1
42	5 1 4	16	5 1 4	8	1
46	3 1 6	16	3 1 6	8	1
50	5 5 0	4	5 5 0	4	1
50	5 3 4	16	5 3 4	8	1
50	7 1 0	8	7 1 0	8	1
54	5 5 2	8	5 5 2	4	1
54	3 3 6	8	3 3 6	4	1
58	7 3 0	8	7 3 0	8	1
66	5 5 4	8	5 5 4	4	1
54	7 1 2	16	7 1 2	8	0.409283
62	7 3 2	16	7 3 2	8	0.409283
66	1 1 8	8	1 1 8	4	0.800909
82	9 1 0	8	9 1 0	8	0.800909
86	9 1 2	16	9 1 2	8	0.800909

[a] Crystal bulk
[b] Crystal surface

electrons, consisting of the excess (vacancy-trapped) electrons, plus those associated with the nearest and next nearest neighbor ions. These molecular clusters were then embedded in a lattice of point ions of charges ±*e* for silver and halides.

The adsorption energy E_{ads} was calculated from the relation

$$E_{ads}=E_{complex}-E_{adsorbate}-E_{substrate} \quad (1)$$

The terms appearing on the right-hand side are the total energies of the complex (adsorbate+substrate), the adsorbate (Ag_2, Ag_2^{2+}, O, O^- or O^{2-}) and the substrate (M-defect-containing surface of AgBr or AgCl), obtained from three independent calculations using the same supercell. The negative adsorption energy E_{ads} indicates that the bound adsorbate is electronically stable.

Density functional theory (DFT) calculations were performed using Becke's three-parameter exchange functional (B3) with the Lee–Yang–Parr (LYP) correlation functional. [20] The Stevens–Basch–Krauss effective core potential (ECP) triple-split basis set CEP-121G [21] with ECPs for Ag, Br and Cl was employed and the calculations were carried out using Gaussian 98. [22]

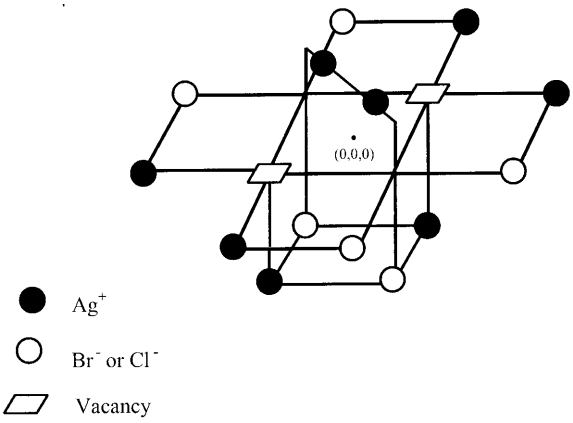

Fig. 2 The Ag_8Br_6 and Ag_8Cl_6 clusters simulating the M-centers on AgBr and AgCl (001) surfaces

Results and discussion

An Ag_2 cluster formed on photo-or chemically reduced silver bromide or chloride surfaces is proposed to be a primary center for latent image formation. [1, 2] Shelimov et al. [7] suggested a mechanism for Ag_2 cluster formation by proposing that in the two-electron reduction process there are two Br atoms removed from adjacent anion sites of the AgBr (100) surface. As a result, two adjacent *F*-centers are formed on the surface. The interactions of these *F*-centers produce a structure referred to as an M-center. This structure may be considered as an Ag_2 molecule adsorbed in a "pit" on the AgBr (100) surface. Here, we apply the same proposal to AgBr and AgCl surfaces using more accurate crystal simulations, DFT calculations level and basis sets and concentrate on two rather different features: First, we optimize the Ag_2 clusters over AgBr and AgCl surfaces for several orientations ranging from the original Ag_2 orientation to the M-center orientation along the ⟨110⟩ axis to assign the most energetically preferred configuration as well as the activation barriers for rotational diffusion. Second, we examine the extent of reduction of the Ag_2 cluster by the two M-center electrons – internal reduction – and by O, O^- and O^{2-} adsorbates as external reducing agents of variable electron donating powers – external reduction- in addition to the nature of adsorbate–substrate interactions. We also draw attention to some of the essential differences between the two halide surfaces.

The AgBr and AgCl clusters simulating the M-centers on AgBr and AgCl surfaces are given in Fig. 2. The energy characteristics of silver clusters over AgBr and AgCl (001) surfaces are given in Table 2. The adsorption energies of Ag_2 and Ag_2^{2+} were calculated to study the mobility of silver clusters adsorbed in the "pit" on the surface under the effect of M-center imperfection (the most stable orientation) and to examine whether the rotation of the adsorbed clusters has any relation to redox reactions. Moreover, Ag_2^{2+} is unstable and it may be interesting to examine its stability over the M-defect-containing surfaces. The bond lengths used for the Ag_2 and

Table 2 Energy characteristics of Ag_2 clusters over AgBr(001) and AgCl (001) surfaces as functions of the rotational angle (θ) in degrees. Total energy E_{tot}, optimal adsorption energies of Ag_2 E_{ads} (Ag_2) and Ag_2^{2+} E_{ads} (Ag_2^{2+}), optimal Ag–Ag, Ag_2/AgBr and Ag_2/AgCl distances R_{Ag2}, R_{Ag2}/AgBr and R_{Ag2}/AgCl. Upper figures refer to AgBr and lower figures to AgCl. All energies are given in Hartrees and distances in ångströms

Rotation angle (θ) (degrees)	E_{tot}	E_{ads} (Ag_2)	E_{ads} (Ag_2^{2+})	R_{Ag2}	$R_{Ag2/AgBr}$ $R_{Ag2/AgCl}$
0	–1271.748607	–0.019765	–0.818532	2.67003	0.19
	–1281.823789	–0.048653	–0.846354	2.68840	0.16
15	–1271.749065	–0.020223	–0.81899	2.67003	0.06
	–1281.824489	–0.050089	–0.844207	2.72732	0.06
30	–1271.749624	–0.021481	–0.816778	2.71655	0.05
	–1281.825355	–0.051899	–0.842730	2.76628	0.05
45	–1271.747049	–0.020967	–0.809432	2.7976	–0.007
	–1281.822027	–0.048570	–0.839408	2.76628	–0.005
60	–1271.741299	–0.015217	–0.803683	2.79760	–0.01
	–1281.815461	–0.042005	–0.832842	2.76628	–0.06
75	–1271.737538	–0.012681	–0.797780	2.83819	0.018
	–1281.812185	–0.038672	–0.829509	2.76628	0.01
90	–1271.736405	–0.011604	–0.796702	2.83819	0.01
	–1281.811969	–0.040818	–0.825152	2.84430	0.016

Ag_2^{2+} dissociation products are the optimal bond lengths given in Table 2 (R_{Ag2}). According to the E_{ads} equation, $E_{ads}(Ag_2)$ and $E_{ads}(Ag_2^{2+})$ differ only by the definition of the dissociation products. The rotational angle of an Ag_2 cluster about an imaginary axis normal to the surface and passing through the origin of the Cartesian coordinates (0,0,0) was varied from 0° (original Ag–Ag orientation) to 90° (M-center orientation) in steps of 15°. The total energies E_{tot} and the adsorption energies of Ag_2 on an M^{2+}-center and Ag_2^{2+}on an M-center – $E_{ads.}(Ag_2)$ and $E_{ads.}$ (Ag_2^{2+}) – respectively, are given in Hartrees. Full optimization of the geometrical parameters, the internuclear separation R_{Ag2} and the adsorbate-substrate distance $R_{Ag2/AgBr}$ or $R_{Ag2/AgCl}$ was carried out for all θ values. The uncertainty of θ was calculated to be ±2°. The optimal total energies E_{tot} (with simultaneous optimization of $R_{Ag–Ag}$ and $R_{Ag2/AgBr}$) at θ=28° and 30° were calculated to be –1271.749544 and –1271.74956 E_h, respectively. Similar uncertainty is expected over the AgCl surface. As shown in Table 2, based on E_{tot} values, the most energetically preferred orientation of Ag_2 clusters is at a rotational angle 30°, 0.05 Å above the surface with internuclear separations of ca. 2.72 Å for AgBr and ca. 2.77 Å for AgCl. The Ag_2/AgCl interactions are stronger than Ag_2/AgBr interactions and while there were no activation barriers for the rotational diffusion of Ag_2 from θ=0°–30°, activation barriers for the rotational diffusion from the equilibrium configuration (θ=30°) to the 90° configuration exist. These were calculated to be ca. 0.360 eV over AgBr surface and ca. 0.364 eV over AgCl surfaces. These activation energies are, as shown, small and close and point to the high mobility of Ag_2 clusters over the surfaces examined.

In Table 2, since $E_{ads}(Ag_2^{2+})$ is always more negative than $E_{ads}(Ag_2)$, we may suggest that silver clusters are not bound to the surface as neutral silver species, but as silver species carrying partial positive charges. The crucial point here is the extent of charge transfer from the M-center to the cluster. To investigate the magnitude of the partial positive charges of these silver clusters, we collected the results of Mulliken population analyses on the defect-free and M-defect-containing surfaces of AgBr and AgCl in Table 3. As shown in this table, ca. 50% of the reduction of silver clusters comes from the surrounding anions and ca. 30–33% from the two electrons of the M-center. So, ca. 80–83% of the reduction of the silver cluster is attributed to the internal or self-reduction, leaving ca. 17–20% for external reduction, i.e. reduction from external sources such as adsorbates and chemical reducing agents or developers. If this is the only factor that contributes significantly to the sensitivity of visible image formation, we may state that both AgBr and AgCl are of comparable sensitivity before M-center formation. However, after M-center formation, the charges of silver clusters over AgCl were significantly smaller than those over AgBr. One possible explanation is that the nearest neighbor Cl^- ions tend to draw the two electrons of the M-center more effectively toward the silver cluster than the less electronegative Br^- ions. From Table 2, we also observe that the rotation of silver clusters over the two silver halide surfaces has no obvious relation to the redox reactions.

Table 3 The magnitude of Mulliken charges on each of the two Ag^+ ions in Ag_2^{2+} clusters over AgBr and AgCl defect-free and defect-containing surfaces. Upper figures refer to AgBr and lower figures to AgCl

Substrate	Charge
$Br_2Ag_8Br_6$	0.504
$Cl_2Ag_8Cl_6$	0.496
M-Ag_8Br_6	0.202
M-Ag_8Cl_6	0.157
M-$Ag_2Ag_6Br_6$[a]	0.200
M-$Ag_2Ag_6Cl_6$[a]	0.148

[a] The optimal orientation of Ag_2^{2+} cluster at θ =30°

In order to understand the possible electrostatic contributions to adsorbate–substrate interactions when using

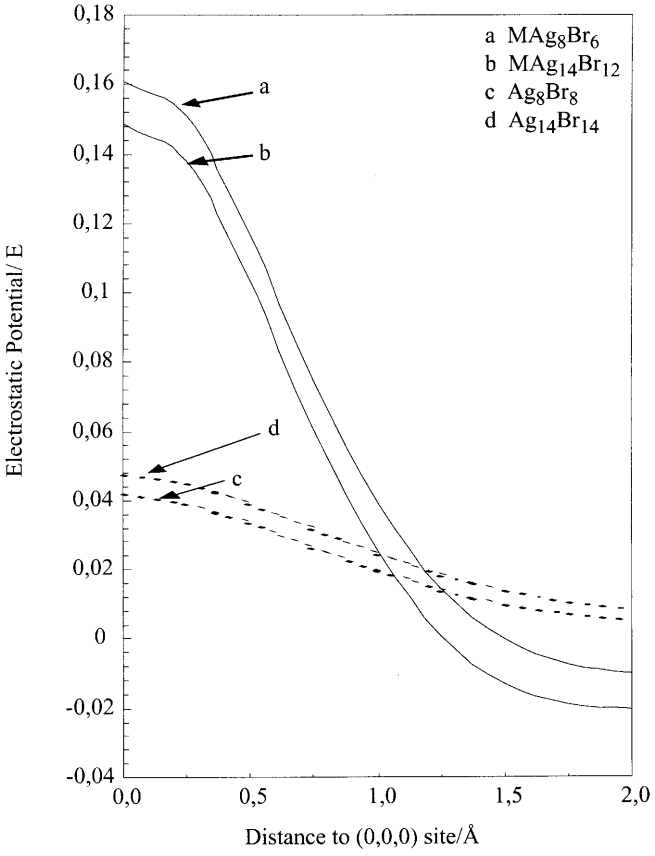

Fig. 3 Electrostatic potentials as a function of the distance to the (0,0,0) site of AgBr defect-free and defect-containing surfaces

defect-free and defect-containing clusters of variable sizes, plus the corresponding embedding at the surface, we calculated the electrostatic potentials over the (0,0,0) site. For AgBr defect-containing surfaces, we selected the most energetically preferred orientation (θ=30°). Figure 3 shows that the electrostatic potentials of clusters that differ in size are quite close and the shapes of the functions are quite similar. On the other hand, the electrostatic potentials of defect-free and defect-containing clusters of the same size are very different and the shapes of the functions are very dissimilar. This implies that we can expect almost the same electric fields and electric field derivatives for larger clusters, defect free or defect containing, while this would not be the case when comparing defect-free with defect-containing clusters of the same size. In other words, the adatom–surface interactions would not be too sensitive to cluster size. On the other hand, since the electrostatic interactions of an adatom with the surface will mainly consist of electric field-induced dipole and electric field derivatives-induced quadrupole moments, one expects that, while the classical contributions to the adatom–surface interactions are quite similar for larger clusters, they are quite different when going from defect-free to defect-containing surfaces. However, curve crossings that occur at adsorbate–substrate distances of ca. 1.0 Å imply that the electrostatic interactions are identical regardless of the cluster size or M-center formation. The results obtained for AgCl were very close to those for AgBr.

Table 4 Optimal adsorbate–substrate distances R_e, and adsorption energies E_{ads} of O, O^- and O^{2-} on AgBr and AgCl defect-containing surfaces (center of mass of silver clusters at θ=30°). Upper figures refer to AgBr and lower figures to AgCl. All distances are given in ångströms and energies in E_h

Adsorbate	R_e	E_{ads}
O	1.60	–0.169965 –0.171106
O^-	1.64	–0.138280 –0.124385
O^{2-}	1.65	–0.511487 –0.482316

Since accidental exposure of photographic materials to atmospheric O, O^- and O^{2-} species – as reducing agents – is probable, we attempted to shed some light on their interactions (adsorption energies and redox reactions) over AgBr and AgCl defect-containing surfaces. The free O^{2-} species is unstable and its stability over the defect-containing surfaces may be of interest. The distance between the adsorbate (O, O^-, O^2) and the substrate surface (center of mass of silver cluster at θ=30° orientation), namely R_e, was optimized and the adsorption energy E_{ads} was calculated in each case. The corresponding data are collected in Table 4. As shown in this table, atomic O adsorbs more stably than O^-, and the dianion O^{2-} dominates the interactions on both surfaces. A strong adsorbate–substrate interaction is observed in each case, so that avoiding long-term exposure to the atmosphere may be taken into account. On the other hand, oxygens are usually considered to take part only in Brϕnsted acid/base reactions where protons are exchanged between surface hydroxyl groups and other reactants. The incoming O species readily accepts charge; the electron affinity of an oxygen atom is 1.462 eV, [23] and it dislikes donating. [24] One therefore expects the oxygen atom to form a strong bond with the surface if the surface is able to donate charge. We have therefore collected the charges of silver clusters on the defect-containing surfaces as well as the charges of O, O^- and O^{2-} in Table 5. As shown in this table, charge transfers from the substrate surface to atomic oxygen as expected. However, for the less electronegative species O^- and O^{2-}, charge transfer takes place from the adsorbate to the substrate surface. Since the adsorptivity of O^{2-} is significantly greater than that of O^-, and O^{2-} is a better electron donor than O^-, the strength of adsorbate–substrate interactions may be related to the electron-donating power of negatively charged adsorbates. However, inspection of Tables 4 and 5 confirms that the total amount of charge transferred between adsorbate and substrate surface is a monotonically increasing function of the adsorption energy.

Reduction of silver ions in contact with any of the practical developers is thermodynamically favored. [25]

Table 5 Charges on O, O^-, O^{2-} and Ag^+ (charge per Ag^+ in Ag^+–Ag^+ pair) of the considered adsorbate–substrate complexes of AgBr and AgCl using R_e values of Table 4 for O^{n-}/M-defect-containing surfaces

Complex[a]	Charges	
$O/MAg_2Ag_6Br_6$	O	–0.532786
	Ag^+–Ag^+	0.358395
$O/MAg_2Ag_6Cl_6$	O	–0.553465
	Ag^+–Ag^+	0.299933
$O^-/MAg_2Ag_6Br_6$	O^-	–0.562823
	Ag^+–Ag^+	0.330431
$O^-/MAg_2Ag_6Cl_6$	O^-	–0.563380
	Ag^+–Ag^+	0.239993
$O^{2-}/MAg_2Ag_6Br_6$	O^{2-}	–0.616645
	Ag^+–Ag^+	0.330974
$O^{2-}/MAg_2Ag_6Cl_6$	O^{2-}	–0.627845
	Ag^+–Ag^+	0.219244

[a] The optimal orientation of Ag_2^{2+} cluster at θ =30°

The electron from a developer molecule is higher in energy and therefore readily transfers to the lowest vacant 5*s* orbital of a silver ion in solution. However, when such a silver ion is incorporated into an ionic crystal, all of its energy levels are raised by several electronvolts by virtue of the Madelung potential at the cation site. In the silver halides the vacant 5*s* level is the origin of the conduction band of the crystal. The conduction band energy minimum is well above the chemical potential range of any non-fogging photographic developer. Electron transfer to the perfect crystal is therefore energetically unfavorable. [1] However, since the Fermi energy of metallic silver lies below the range of chemical potentials of working developers – and thus charge transfer to silver metal is favored – we can expect a competition between developers and atmospheric adsorbates. If so, chemical reducing agents should be selected so that their reduction potentials must be significantly greater than any of the probable atmospheric adsorbates.

To clarify the directions of charge transfer between the free adsorbates and the AgBr surface, we have calculated the corresponding energy levels of each species (Fig. 4). In this figure, the directions of charge transfer are represented by the three arrows marked 1, 2 and 3. In other words, while the O species acts as an electron acceptor, O^- and O^{2-} act as electron donors. On the other hand, the band gaps of the defect-free and defect-containing surfaces (calculated as the differences between the valence and conduction bands) suggest that M-center imperfection (M-Ag_8Br_6, θ=30°) changes the nature of the AgBr surface from an insulator (band gap=4.38 eV) to a semiconductor (band gap=1.76 eV) and therefore enhances the electrical properties of the surface. We also note that, since the present cluster models do consider the Madelung potentials representing the ions in the rest of the crystal, because they are regarded as a part of the solid, the calculated band gap narrowing is not exaggerated. The results obtained for AgCl were very close to those for AgBr.

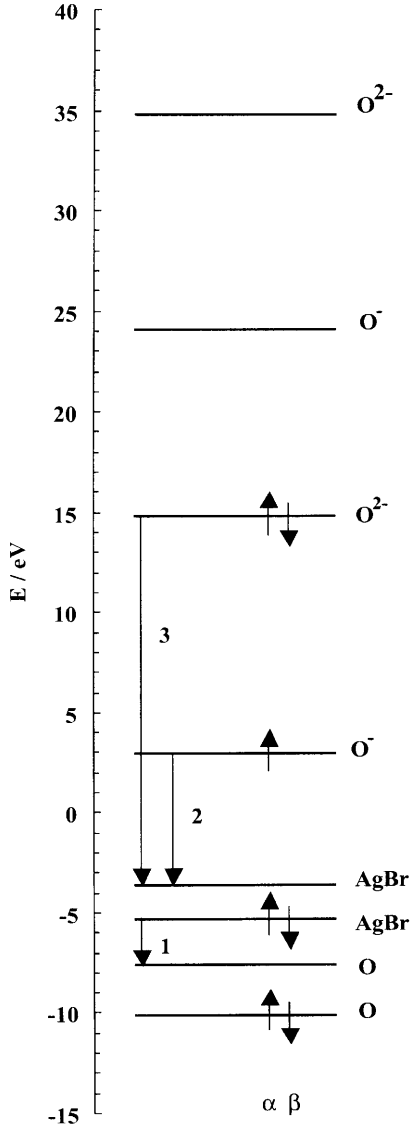

Fig. 4 The tops of valence bands and the bottoms of conduction bands of O, O- and O^{2-} adsorbates and AgBr defect-containing surface M-Ag8Br6 (θ=30°)

Conclusions

In the present study, an attempt has been made to provide a model for latent-image formation in the photographic process in addition to related surface properties such as barriers of Ag_2 rotation and O^{n-} adsorption.

The most energetically preferred orientation of silver clusters and the allowed percentages of reduction at the relevant surfaces were estimated and light has been shed on the redox reactions of O^{n-} adsorbates. No remarkable differences were observed between the two alkali halide surfaces in terms of reduction and mobility of silver clusters or stability of adsorbates. It turns out that the photographic sensitivity of each substrate is close to the second under the effect of M-center imperfection.

A search for other defect-based models of latent image formation may be suggested for optimal selection of defects that have desirable properties for latent image formation.

References

1. Hamilton JF (1988) Adv Phys 37:359
2. James TM (1984) The theory of the photographic process. In: Baldereschi A, Czaja W (eds) Proceeding of the Third Trieste Symposium on the Physics of Latent Image Formation in Silver Halides, Trieste, 1983. World Scientific, Singapore
3. (a) Baetzold RC (1973) Photogr Sci Eng 19:11; (b) Baetzold RC (1980) Photogr Sci Eng 28:15
4. Jacobs PWM, Corish J, Catlow CRA (1980) J Phys C 13:1977
5. Flad J, Stoll H, Preuss H (1987) Z Phys D 6:193
6. Flad J, Stoll H, Preuss H (1987) Z Phys D 6:287
7. Shelimov KB, Safonov AA, Bagatur'yants AA (1993) Chem Phys Lett 201:84
8. (a) Mejias JA (1996) Phys Rev B 53:10281, (b) Shalabi AS, El Mahdy AM, Kamel MA, Ismail GH (2000) J Phys Chem Solids 61:1415
9. Wimmer E, Fu CL, Freeman AJ (1985) Phys Rev Lett 55:2618
10. Colbourn EA (1991) Rev Solid State Sci 5:91
11. (a) Johnson KH, Pepper SV (1982) J Appl Phys 53:6634; (b) Anderson AB, Ravimohan C, Mehandru SP (1987) Surf Sci 183:435; (c) Horsley JA (1979) J Am Ceram Soc 101:2870
12. Evjen HM (1932) Phys Rev 39:675
13. Harris FE (1975) In: Eyring H, Henderson D (eds) Theoretical chemistry: advances and perspectives, vol. I. Academic Press, New York
14. Colbourn EA (1991) Rev Solid State Sci 5:391
15. Colbourn EA (1989) In: Catlow CRA (ed) Advances in solid state chemistry, Vol 1. JAI Press, London
16. Surrat GT, Kunz AB (1978) Phys Rev Lett 40:347
17. Colbourn EA, Mackrodt WC (1982) Surf Sci 117:571
18. Shalabi AS, Mahdy AME (1999) J Phys Chem Solids 60:305
19. Shalabi AS, Assem MM, Abdel Aal S, Kamel MA, Abdel Rahman MM (1999) Solid State Commun 111:735
20. Becke AD (1993) J Chem Phys 98:5648
21. (a) Stevens W, Basch H, Krauss J (1984) J Chem Phys 81:6026; (b) Stevens W, Krauss M, Basch H, Jasien PG (1992) Can J Chem 70:612; (c) Cundari TR, Stevens WJ (1993) J Chem Phys 98:5555
22. Frisch MJ, Trucks GW, Schlegel HB, Scuseria GE, Robb MA, Cheeseman JR, Zakrzewski VG, Montgomery JA, Stratman RE, Burant JC, Dapprich S, Millam JM, Daniels AD, Kudin KN, Strain MC, Farkas O, Tomasi J, Barone V, Cossi M, Cammi R, Mennucci B, Pomelli C, Adamo C, Clifford S, Ochterski J, Petersson GA, Ayala PY, Cui Q, Morokuma K, Malick DK, Rabuck AD, Raghavachari K, Foresman JB, Cioslowski J, Ortiz JV, Baboul AG, Stefanov BB, Liu C, Liashenko A, Piskorz P, Komaromi, I, Gomperts R, Martin RL, Fox DJ, Keith T, Al-Laham MA, Peng CY, Nanayakkara A, Gonzalez C, Challacombe M, Gill PMW, Johnson BG, Chen W, Wong MW, Andres JL, Gonzales C, Head-Gordon M, Replogle ES, Pople JA (1998) Gaussian 98. Gaussian, Pittsburgh Pa.
23. Strömberg D (1992) Surf Sci 275:473
24. Nygren MA, Pettersson LGM (1994) Chem Phys Lett 230:456
25. Hamano H, Ari G (1979) J Photogr Sci 27:17, 241